Article

Cyanide Addition to Diiron and Diruthenium Bis-Cyclopentadienyl Complexes with Bridging Hydrocarbyl Ligands

Alessia Cinci [1], Gianluca Ciancaleoni [1], Stefano Zacchini [2] and Fabio Marchetti [1,*]

[1] Department of Chemistry and Industrial Chemistry, University of Pisa, Via G. Moruzzi 13, I-56124 Pisa, Italy
[2] Department of Industrial Chemistry "Toso Montanari", University of Bologna, Via P. Gobetti 85, I-40129 Bologna, Italy; stefano.zacchini@unibo.it
[*] Correspondence: fabio.marchetti@unipi.it

Abstract: We conducted a joint synthetic, spectroscopic and computational study to explore the reactivity towards cyanide (from Bu_4NCN) of a series of dinuclear complexes based on the $M_2Cp_2(CO)_3$ scaffold (M = Fe, Ru; Cp = η^5-C_5H_5), namely $[M_2Cp_2(CO)_2(\mu$-$CO)\{\mu,\eta^1:\eta^2$-$CH=C=CMe_2\}]BF_4$ (**1Fe-Ru**), $[Ru_2Cp_2(CO)_2(\mu$-$CO)\{\mu,\eta^1:\eta^2$-$C(Ph)=CHPh\}]BF_4$ (**2Ru**) and $[M_2Cp_2(CO)_2(\mu$-$CO)\{\mu$-$CN(Me)(R)\}]$ CF_3SO_3 (**3Fe-Ru**). While the reaction of **1Fe** with Bu_4NCN resulted in prevalent allenyl deprotonation, preliminary CO-NCMe substitution in **1Ru** enabled cyanide addition to both the allenyl ligand (resulting in the formation of a h^1:h^2-allene derivative, **5A**) and the two metal centers (affording **5B1** and **5B2**). The mixture of **5B1-2** was rapidly converted into **5A** in heptane solution at 100 °C, with **5A** being isolated with a total yield of 60%. Following carbonyl-chloride substitution in **2Ru**, CN^- was incorporated as a terminal ligand upon Cl^- displacement, to give the alkenyl complex **6** (84%). The reactivity of **3Fe** and **3Ru** is strongly influenced by both the metal element, M, and the aminocarbyne substituent, R. Thus, **7aRu** was obtained with a 74% yield from cyanide attack on the carbyne in **3aRu** (R = Cy, cyclohexyl), whereas the reaction involving the diiron counterpart **3aFe** yielded an unclean mixture of the metastable **7aFe** and the CO/CN^- substitution product **8aFe**. The cyano-alkylidene complexes **7aRu** (R = Cy) and **7bFe** (R = Me) underwent CO loss and carbene to carbyne conversion in isopropanol at 60–80 °C, giving **8aRu** (48%) and **8bFe** (71%), respectively. The novel compounds **5A**, **5B1-2**, **6** and **7aRu** were characterized by IR and NMR spectroscopy, with the structure of **7aRu** further elucidated by single crystal X-ray diffraction analysis. Additionally, the DFT-optimized structures of potential isomers of **5A**, **5B1-2** and **6** were calculated.

Keywords: organometallic chemistry; dimetallic complexes; allenyl ligand; alkenyl ligand; carbyne ligand; cyanide addition

1. Introduction

Dinuclear metal complexes enable unique reactivity patterns on bridging ligands, arising from the cooperativity of the two closely situated metal centers, which are generally not attainable in related mononuclear species [1–5]. The readily available and cost-effective diiron compound $[Fe_2Cp_2(CO)_4]$ (Cp = η^5-C_5H_5) serves as an ideal platform to explore this chemistry, and it has indeed been utilized as a starting material to build a diverse array of bridging organometallic architectures [6–10]. Typically, these reaction pathways initiate with the substitution of one carbonyl ligand, induced by either thermal or photolytic treatment. The parallel reactivity of the diruthenium homolog $[Ru_2Cp_2(CO)_4]$, though relatively less explored, exhibits substantial similarities compared to its diiron counterpart. However, the stronger Ru-Ru bond, compared to Fe-Fe, permits, in specific cases, the modification of bridging hydrocarbyl fragments, avoiding detrimental fragmentation pathways that may be favored with the diiron complexes (vide infra) [11]. Notably, the benchmark organometallic species $[M_2Cp_2(CO)_4]$ (M = Fe, Ru) has been extensively studied in the past decades to explore new routes for carbon–carbon bond formation, aiming to

model the heterogeneously catalyzed Fischer–Tropsch process [6,12–14]. Essentially, these studies relied on the principle that a dimetallic framework may represent the simplest system suitable for modeling a metal surface [15].

The present work focuses on the reactivity of selected derivatives of $[M_2Cp_2(CO)_4]$ (M = Fe, Ru) featuring distinct hydrocarbyl ligands occupying a bridging coordination site, namely allenyl (**1**), alkenyl (**2**) and aminocarbyne (**3**), see Scheme 1. These air-stable compounds can be prepared using synthetic methodologies involving the initial displacement of one CO ligand with, respectively, 2-methyl-3-butyn-2-ol (leading to **1Fe-Ru** [16,17]), diphenylacetylene (**2Ru** [18,19]) and isocyanides CNR (**3Fe-Ru** [20–22]).
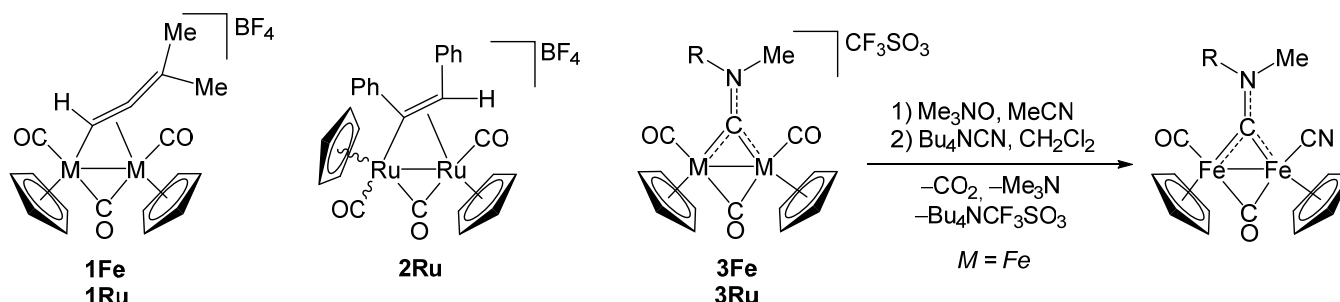
Scheme 1. Diruthenium and diiron complexes sharing the $M_2Cp_2(CO)_3$ core with different hydrocarbyl ligands on a bridging position, and synthesis of diiron aminocarbyne cyanide complexes via TMNO strategy [R = Me, CH_2Ph (benzyl), Xyl = $2,6\text{-}C_6H_4Me_2$ (meta-xylyl), $4\text{-}C_6H_4OMe$, Cy = C_6H_{11} (cyclohexyl), $CHCH=CH_2$ (allyl)].

The diruthenium allenyl complex **1Ru** exhibits a rich and versatile reactivity once a coordination site becomes available. This can be achieved using trimethylamine N-oxide (Me_3NO = TMNO) in acetonitrile as a typical solvent, resulting in the selective substitution of one CO (eliminated as CO_2) with a labile NCMe ligand [23,24]. This lability is equivalent to a coordination vacancy, facilitating the entry of unsaturated substrates (e.g., alkynes, alkenes), which then couple with the bridging hydrocarbyl ligand to generate diverse organometallic motifs [25,26]. However, the parallel chemistry of **1Fe** is not accessible due to prevalent Fe-Fe bond cleavage induced by CO removal (see above) [16]. Similar considerations apply to related alkenyl complexes, with the diruthenium **2Ru** (and similar compounds) providing access to diverse structures upon reaction with small unsaturated organic units [27,28]. Concerning the aminocarbyne complexes, **3Fe** can be easily obtained, even in multigram scales, exploiting a straightforward and quite general synthetic route [20,21]. The successive CO-NCMe substitution takes place with preservation of the dinuclear structure, allowing for several derivatization reactions that have been documented in the literature [7,8]. Conversely, the synthesis of diruthenium aminocarbyne complexes (**3Ru**) is more challenging, and the N-cyclohexyl derivative (R = Cy in Figure 1) is the only one producible in a scale practically suitable for exploratory chemistry [22].

Cyanide addition serves as a valuable strategy for generating C-C bonds in organometallic chemistry [29,30], with tetrabutylammonium cyanide (Bu_4NCN) being a convenient reagent due to its good solubility in common organic solvents [31,32]. To date, the reactivity of diiron and diruthenium μ-allenyl and μ-alkenyl complexes (**1–2**, and their acetonitrile derivatives) with Bu_4NCN remains unexplored. Conversely, this chemistry has been investigated for a few compounds of type **3**, showing a significant influence of the specific R substituent [20,33,34]. Moreover, diiron derivatives with a terminal cyanide ligand can be prepared from **3Fe** in two steps, via the intermediate formation of labile acetonitrile adducts (Scheme 1) [35,36].
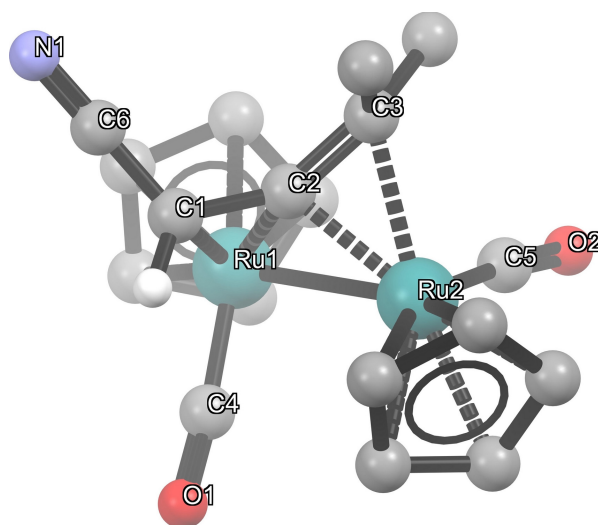
Figure 1. DFT-optimized geometry of the most stable isomer of **5A** (**5A-is1**, see also Figure S1). Hydrogen atoms, except $C_\alpha H$, have been omitted for clarity. Selected computed bond lengths (Å) and angles (°): Ru1-C4 1.852, C4-O1 1.171, Ru2-C5 1.843, C5-O2 1.172, Ru1-C1 2.217, Ru1-C2 2.043, Ru2-C2 2.046, Ru2-C3 2.299, C1-C2 1.438, C2-C3 1.415, C1-C6 1.428, C6-N1 1.170, C1-C6-N1 179.58, C1-C2-C3 139.63, Ru1-C4-O1 172.54, Ru2-C5-O2 173.13, Ru1-C2-Ru2 91.39, C1-C2-Ru2 125.82, C3-C2-Ru1 137.80.

Expanding our understanding of the reactivity of **1**–**3** with cyanide is motivated by two primary reasons. First, the unsaturation within the bridging hydrocarbyl ligand offers opportunities to increase the complexity of the organic moiety [37–39], with the cyano group potentially acting as a nitrogen donor towards one of the two iron centers [40–42]. Second, the possibility of placing cyanide to occupy an iron coordination site deserves consideration for potential implications in catalysis [43]. In particular, previous studies have shown that diiron bis-cyclopentadienyl complexes with terminal cyanide and bridging carbyne ligands behave as models of [FeFe] hydrogenase [44,45], promoting the electrocatalytic production of dihydrogen from acetic acid [46]. It is hypothesized that the unsaturated carbon (carbyne) and nitrogen (CN) carbons bind the hydrogen atoms prior to H-H bond formation [47,48]. Herein, we present a synthetic, spectroscopic and computational study providing new insights into the chemistry of **1**–**3**, and some of their related acetonitrile derivatives, with Bu_4NCN.

2. Results and Discussion

We started investigating the reactivity of the diiron allenyl complex **1Fe** with Bu_4NCN. This reaction predominantly yielded the diferracyclopentenone complex **4**, resulting from the deprotonation of one methyl group [16] (Scheme 2). Given the ability of the cyanide ion to behave as a Brønsted base towards the allenyl ligand, we turned our attention to the acetonitrile derivative **1Ru-NCMe**, which was prepared from **1Ru** using the literature procedure [25]. The subsequent reaction with Bu_4NCN produced a mixture of products (Scheme 2), which could be partially separated via careful column chromatography on alumina.

The first fraction eluted was complex **5A**, comprising a $\mu\text{-}\eta^2\text{:}\eta^2$ coordinated allene ligand resulting from CN^- addition to the α carbon of the allenyl moiety. This product was isolated with a yield of approximately 30% and identified by IR and NMR spectroscopy. The infrared spectrum of **5A** (in CH_2Cl_2 solution) exhibits the characteristic pattern of analogous diruthenium and diiron compounds [49,50], with two bands ascribable to the terminal carbonyls falling at 1948 and 1927 cm^{-1}, the latter being more intense than the former. Additionally, the weak absorption at 2200 cm^{-1} accounts for the cyanide incorporated within the allene moiety. The NMR spectra of **5A** (in CDCl$_3$) show two sets of resonances in a molar ratio of 1.7, attributed to the two stereoisomers (**5A-is1** and **5A-is2**) differing in the spatial orientation of the C_α substituents (i.e., CN and H), with the Cp ligands

adopting a mutual trans geometry (with respect to the Ru-Ru axis). Remarkably, the related complex [Ru$_2$Cp$_2$(CO)$_2$\{μ,η^2:η^2-CH$_2$=C=CMe(Ph)\}] was reported to exist in CD$_2$Cl$_2$ solution as two stereoisomers related to the spatial arrangement of Me and Ph [49]. We note that the trans configuration for the Cp rings has been recognized in the solid-state structures of all crystallographically characterized complexes based on the M$_2$Cp$_2$(CO)$_2$ core (Cp = C$_5$H$_5$ or substituted cyclopentadienyl) and containing a bridging (substituted) μallene ligand [50–52].
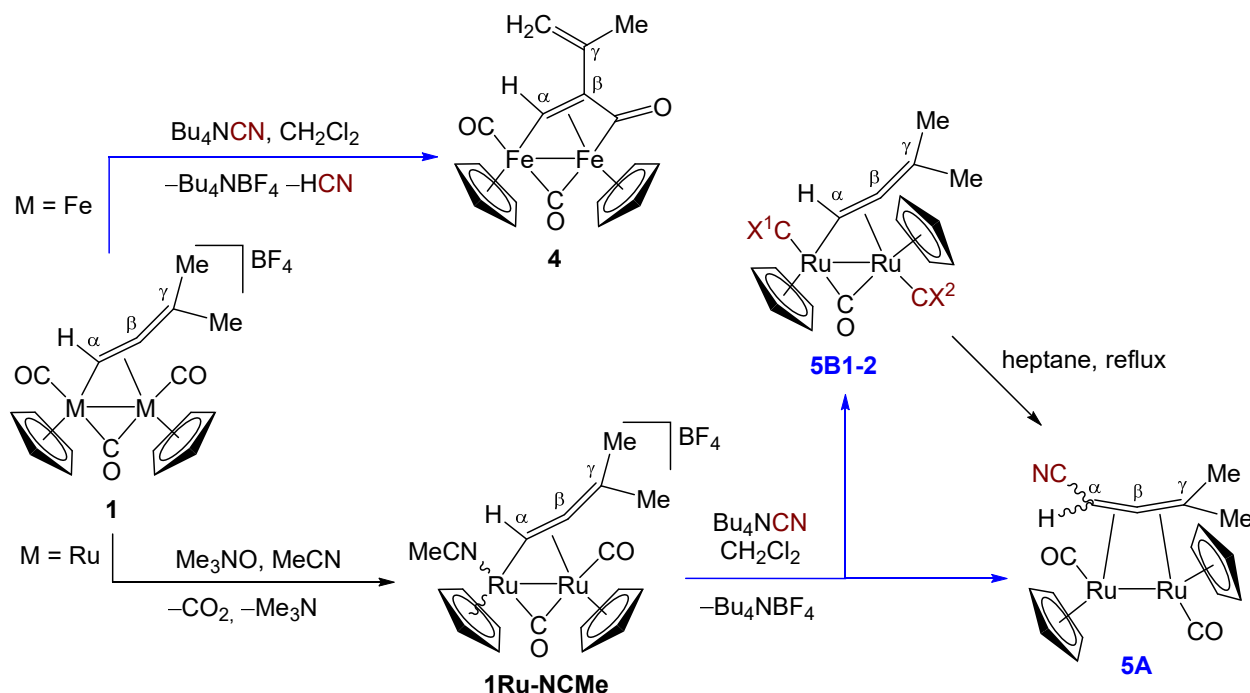

Scheme 2. Reactions of diiron/diruthenium μ-allenyl complexes with tetrabutylammonium cyanide. Novel products/pathways are denoted in blue, while wavy bonds indicate stereoisomers. **5B1**: X^1 = N, X^2 = O; **5B2**: X^1 = O, X^2 = N.

The optimized geometries of **5A-is1** and **5A-is2** were DFT calculated and are shown in Figure S1. The structure with the cyano group pointing far away from the Ru$_2$Cp$_2$ scaffold (**5A-is1**) was found to be more stable than the other one by approximately 1.4 kcal/mol; a view of this structure is depicted in Figure 1 along with the main calculated bonding parameters. The lower stability of the cis configuration for the Cps was confirmed on theoretical grounds (Figure S1).

In agreement with the existence of **5A-is1** and **5A-is2**, the ^{1}H NMR spectrum exhibits the resonance for the C$_\alpha$H hydrogen shifted by ca. 1 ppm in the two isomers (2.47 and 3.45 ppm, respectively). The Cp ligands were detected in the ranges 4.83–5.11 ppm (^{1}H) and 85.9–87.8 ppm (^{13}C). In the ^{13}C NMR spectrum of **5A**, the allene unit gives rise to three diagnostic resonances, at 189.8 (C$_\beta$), 65.4 (C$_\gamma$) and 5.32 ppm (C$_\alpha$), for the prevalent isomer. For comparison, the corresponding signals in the major isomer of [Ru$_2$Cp$_2$(CO)$_2$\{μ,η^2:η^2-CH$_2$=C=CMe(Ph)\}] were observed at 189.9 (C$_\beta$), 62.1 (C$_\gamma$) and 25.0 ppm (C$_\alpha$) [49].

The most abundant fraction collected from the column chromatography of the reaction mixture from **1Ru-NCMe** and Bu$_4$NCN consisted of a mixture of the diruthenium complexes **5B1** and **5B2** (in a ratio of ≈3.3 according to ^{1}H NMR) that could not be separated from the ammonium salt by-product (Scheme 2). The identity of the isomers **5B1** and **5B2** was determined based on IR and ^{1}H NMR spectra, with the assistance of DFT calculations and literature data. In both isomers, the infrared wavenumber for the cyanide group (2104 cm^{-1}) is lowered by ca. 100 cm^{-1} compared to **5A**, indicative of coordination to a low valent ruthenium center [35,53–55]. The predominant isomer (**5B1**, see the DFT-optimized structure in Figure 2) displays one terminal CO (1983 cm^{-1}) and one *semibridging* CO

ligand (1894 cm^{-1}), with the cyano group bound to Ru1 and the Cp ligands adopting a trans configuration. The same geometry was previously recognized for the closely related chloride complex [Ru$_2$Cp$_2$(Cl)(CO)(μ-CO){μ,η^1:η^2-CH=C=CMe$_2$}], **1Ru-Cl** (Figure 2), crystallographically characterized [49]. In the IR spectrum of **1Ru-Cl** (in CH$_2$Cl$_2$), the carbonyl absorptions fall at 1982 and 1882 cm^{-1}. The semibridging coordination of one CO ligand is evident from the computational data obtained for **5B1**, with the Ru1-μCO distance (1.904 Å) considerably shorter than Ru2-μCO (2.376 Å), analogous to what was reported for **1Ru-Cl** [experimental distances of 1.886(3) and 2.403(2) Å, respectively]. Complex **5B2** features the cyanide ligand bound to Ru2, and terminal and classical bridging carbonyl ligands, with corresponding IR stretching vibrations occurring at 1983 and 1827 cm^{-1}. The calculated Ru-μCO bond lengths are 2.022 and 2.083 Å (Figure 2).
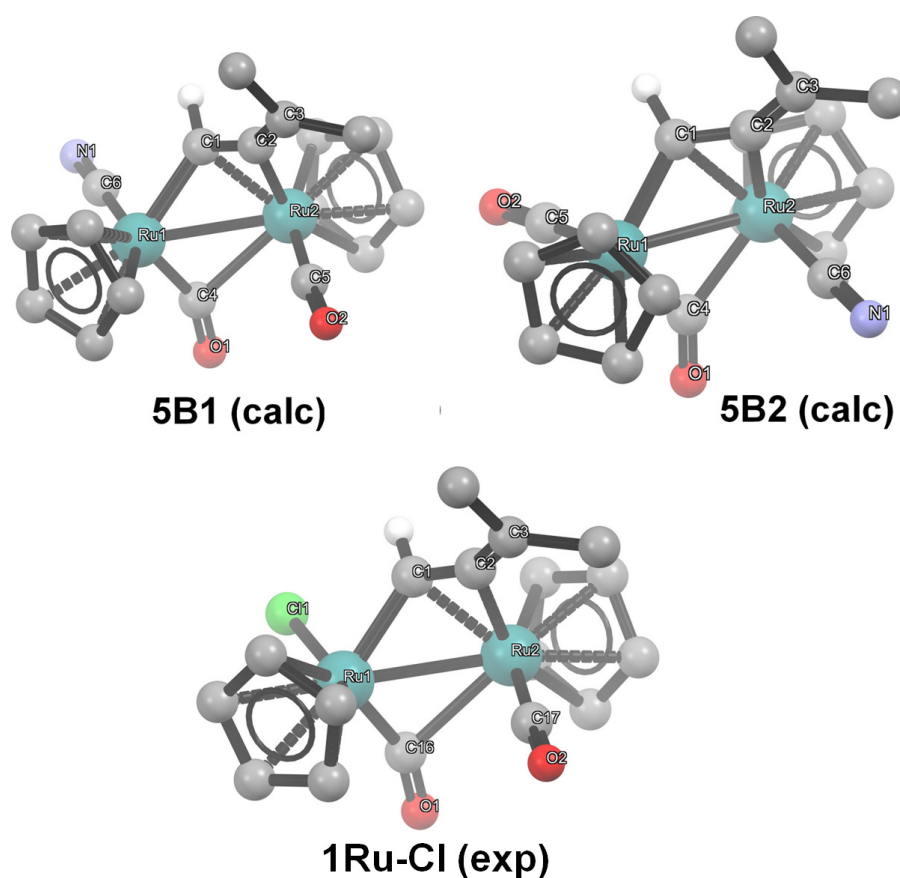
Figure 2. DFT-optimized geometries of **5B1** and **5B2** and X-ray crystal structure of **1Ru-Cl** [49]. Hydrogen atoms (except C$_\alpha$H) have been omitted for clarity. Selected computed bond lengths (Å) and angles (°): **5B1**, Ru1-C6 1.982, Ru1-C4 1.904, C4-O1 1.180, Ru2-C4 2.376, Ru2-C5 1.856, C5-O2 1.164, Ru1-C1 2.059, Ru2-C1 2.151, C6-N1 1.177, C1-C2 1.381, C2-C3 1.335, C1-C2-C3 150.77, Ru1-C1-Ru2 83.79, Ru2-C4-O1 123.33, Ru1-C6-N1 177.96; **5B2**, Ru1-C5 1.845, Ru1-C4 2.022, C4-O1 1.187, Ru2-C4 2.083, Ru2-C6 1.992, C5-O2 1.167, Ru1-C1 2.067, Ru2-C1 2.149, C6-N1 1.177, C1-C2 1.382, C2-C3 1.337, C1-C2-C3 148.27, Ru1-C1-Ru2 82.63, Ru2-C4-Ru1 136.20, Ru2-C6-N1 175.92. Selected experimental bond lengths (Å) and angles (°): **1Ru-Cl**, Ru1-C16 1.886(3), C16-O1 1.162(3), Ru2-C16 2.403(2), Ru2-C17 1.873(2), C17-O2 1.141(3), Ru1-C1 2.031(2), Ru2-C1 2.137(2), C1-C2 1.372(3), C2-C3 1.320(3), C1-C2-C3 152.9(2), Ru1-C1-Ru2 83.66(8), Ru2-C16-O1 122.5(2).

The ^{1}H NMR spectrum of the mixture **5B1/5B2** exhibits the typical low-field resonance for the C$_\alpha$-H (9.06 ppm for **5B1**, 9.44 ppm for **5B2**) [49,56,57], confirming that the structure and coordination of the bridging allenyl ligand are not affected by the incorporation of the cyano group in the complex. The ^{1}H NMR signals for the Cp rings of **5B1-2** fall in the range 5.08 to 5.30 ppm, indicating the same Cp arrangement in these two complexes. Since these

chemical shift values are quite close to those reported for **1Ru-Cl** (4.91, 5.26 ppm) and other trans-$Ru_2Cp_2(CO)_2$ structures with bridging hydrocarbyl ligands [58], it is plausible that the trans geometry occurs in **5B1-2**.

The computed Gibbs free energy difference between trans-**5B1** and trans-**5B2** is small (<1 kcal/mol), justifying the occurrence of both these geometric isomers. However, computer outcomes do not rule out the potential existence of cis structures (see Figure S2).

It appears that the formation of **5A** and **5B1-2** takes place with a rearrangement of the Ru_2Cp_2 core, transitioning from the cis geometry observed in **1Ru** [25] to the trans one. This phenomenon, well described for various CO-substituted bimetallic complexes, is believed to proceed according to the Adams–Cotton mechanism [8,59–61]. In this mechanism, cis and trans isomers may interconvert in solution via a bridge-opened structure, where bridging ligands move to terminal positions, followed by rotation around the metal–metal bond. The coordination switch from terminal to bridging sites and vice versa is likely responsible for the cyanide ligand in **5B1-2** binding to different ruthenium atoms. Notably, fast mobility of cyanide, moving from one metal center to another, was previously observed in $[Fe_2Cp_2(CN)(CO)_3]^-$ [62] and trinuclear platinum clusters [63].

To assess the thermodynamic stability of **5A** and **5B1-2**, we subjected these compounds to heating in heptane solution at ca. 100 °C. While **5A**, and its stereoisomeric ratio, remained unchanged after 2 h, selective conversion of **5B1-2** to **5A** was complete in approximately 10 min. Complex **5A** was subsequently purified by alumina chromatography, providing a total yield of this compound from **1Ru** of 60%. The cyanide migration reaction converting **5B1-2** to **5A** mirrors the migration of hydride from bridging metal coordination to the C_α allenyl carbon in a closely related diruthenium system [49].

The diphenyl-alkenyl diruthenium complex **2Ru-NCMe** was prepared using the TMNO strategy [18], then **2Ru-NCMe** was allowed to react with Bu_4NCN in dichloromethane solution. This reaction cleanly resulted in acetonitrile–cyanide substitution, giving rise to **6** (Scheme 3). However, all our attempts to isolate **6** from tetrabutylammonium tetrafluoroborate, formed as the by-product of the substitution reaction, were unsuccessful. Consequently, an alternative route was devised to obtain pure **6**. Initially, **2Ru-NCMe** was converted to the chloride derivative **2Ru-Cl** following a literature procedure. Subsequently, the reaction of **2Ru-Cl** with Bu_4NCN proceeded smoothly at room temperature affording **6** which could be effectively separated from Bu_4NCl by alumina chromatography. The novel complex **6** was finally isolated with an 84% yield.

According to DFT calculations, the most stable structure of **6** features the cyano group bound to Ru2, with the Cp rings in the trans configuration (Figure 3). The bridging CO ligand is almost equidistant between the two ruthenium centers, the calculated Ru-μCO distances being 2.016 and 2.079 Å. Similarly, the alkenyl C_α carbon is nearly equidistant from the two ruthenium centers, with Ru-C_α distances of 2.097 and 2.169 Å.

Alternative isomers, respectively bearing Cp ligands in cis or the cyano bound to the other ruthenium (Ru1), appear significantly less probable on theoretical grounds (Figure S3). In particular, similar to the μ-allenyl complexes **5B1-2**, the binding of cyanide to Ru1 would force one CO ligand to adopt a semibridging coordination fashion. Computed Ru-μCO distances in trans-**6-1** are 1.902 and 2.347 Å, see Figure S3.

The spectroscopic data collected for **6** are in full agreement with the DFT outcomes. The IR spectrum, recorded in dichloromethane solution, exhibits three main absorptions accounting for a ruthenium-bound cyanide (2104 cm^{-1}), a terminal carbonyl (1978 cm^{-1}) and a bridging carbonyl ligand (1826 cm^{-1}). The NMR spectra reveal a single species in $CDCl_3$ solution, with the Cp rings resonating at 5.38 and 4.97 ppm (^{1}H) and 93.3 and 93.0 ppm (^{13}C). In the ^{1}H spectrum, the alkenic CH appears at 4.92 ppm, while, in the ^{13}C NMR spectrum, the alkenic carbons, C_a and C_b, have been detected, respectively, at 154.4 and 72.4 ppm, and the cyanide at 132.6 ppm. The values for C_a and C_b are quite close to those reported for the crystallographically characterized trans-**2Ru-Cl** [27], and in particular, the low-field chemical shift of C_a aligns with its bridging alkylidene character [7,8,27,64].
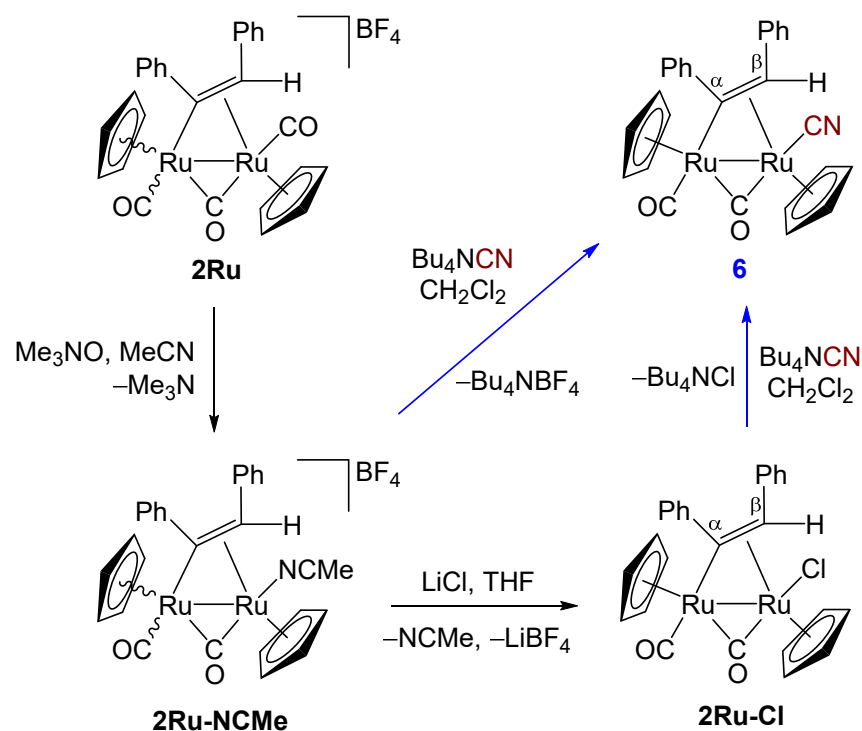
Scheme 3. Synthetic routes leading to a diruthenium μ-alkenyl complex with a cyanide ligand. Novel products/pathways are denoted in blue, while wavy bonds indicate cis-trans isomers.
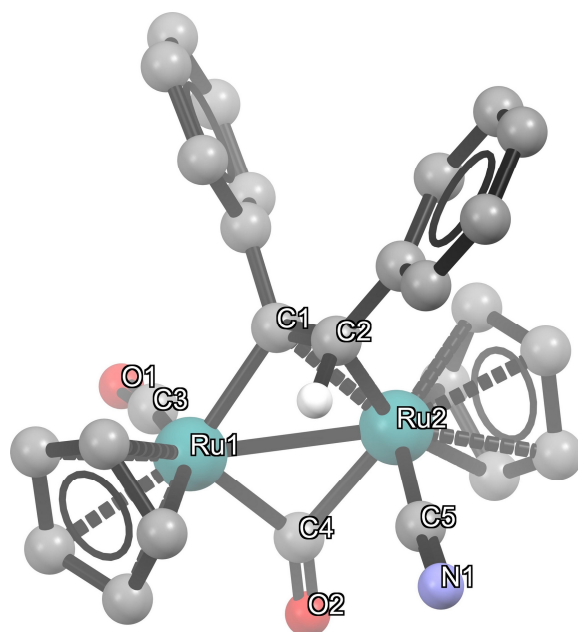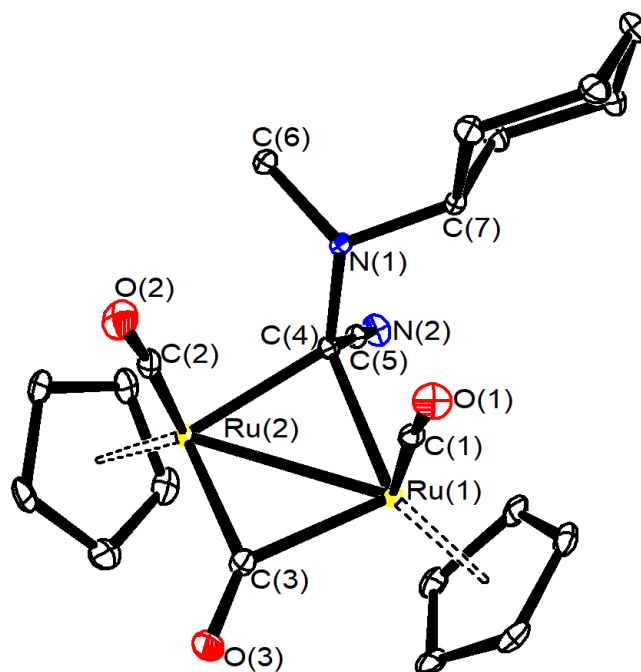

Figure 3. DFT-optimized geometry of **6**. Hydrogen atoms (except the alkenyl CH) have been omitted for clarity. Selected computed bond lengths (Å) and angles (°): Ru1-C3 1.844, Ru1-C4 2.016, C3-O1 1.167, Ru2-C4 2.079, Ru2-C5 1.995, C4-O2 1.187, Ru1-C1 2.097, Ru2-C1 2.169, Ru2-C2 2.284, C5-N1 1.177, C1-C2 1.432, Ru1-C1-C2 113.30, Ru1-C1-Ru2 81.25, Ru2-C4-O2 135.53, Ru2-C5-N1 175.93.

We extended our study to the reactivity of the diiron and diruthenium aminocarbyne complexes **3** with Bu₄NCN (Scheme 4). The reaction involving the diruthenium complex **3aRu** yielded the bridging μalkylidene derivative **7aRu**, resulting from the selective cyanide addition to the carbyne center. This outcome aligns with the previous

reaction involving the N-benzyl substituted homologue of **3aRu**, [Ru$_2$Cp$_2$(CO)$_2$(μ-CO){μ-CN(Me)(CH$_2$Ph)}]CF$_3$SO$_3$, affording [Ru$_2$Cp$_2$(CO)$_2$(μ-CO){μ-C(CN)NMe(CH$_2$Ph)}] [34].

Scheme 4. Reactions of diiron/diruthenium μ-aminocarbyne complexes with tetrabutylammonium cyanide. Novel products/pathways are denoted in blue, while wavy bonds indicate stereoisomers.

Complex **7aRu** was isolated after alumina chromatography and isolated with a 74% yield. X-ray quality crystals of this compound were obtained from a dichloromethane/hexane mixture settled aside at −30 °C, and the molecular structure was subsequently determined through X-ray diffraction analysis (Figure 4). A few dinuclear complexes containing a bridging cyano-aminoalkylidene ligand have been crystallographically characterized, all based on the M$_2$Cp$_2$(CO)$_2$ core (M = Fe, Ru) [34,38,65–68]. Bonding parameters of **7aRu** resemble those previously reported for the closely associated compound [Ru$_2$Cp$_2$(CO)$_2$(μ-CO){μ-C(CN)NMe(CH$_2$Ph)}], featuring a benzyl group in place of cyclohexyl [34]. In both structures, the cyano group points towards the side with the Cp rings, which are in relative *cis* orientation. In **7aRu**, the C(4)-N(1) contact [1.458(4) Å] is almost a pure single bond and, in keeping with this, N(1) strongly departs from sp^2 hybridization [sum angles at N(1) 341.2(5)°]. The bridging μ-CO and μ-C(CN)N(Me)(Cy) ligands are perfectly symmetric [Ru(1)-C(3) 2.041(4), Ru(2)-C(3) 2.014(3), Ru(1)-C(4) 2.098(3), Ru(2)-C(4) 2.098(3) Å] with both Ru atoms bonded to terminal CO ligands.

Figure 4. View of the molecular structure of **7aRu**. Displacement ellipsoids are at the 30% probability level. H-atoms have been omitted for clarity. Main bond distances (Å) and angles (°): Ru(1)-Ru(2) 2.7023(4), Ru(1)-C(1) 1.872(4), Ru(2)-C(2) 1.873(4), Ru(1)-C(3) 2.041(4), Ru(2)-C(3) 2.014(3), Ru(1)-C(4) 2.098(3), Ru(2)-C(4) 2.098(3), C(1)-O(1) 1.146(4), C(2)-O(2) 1.137(4), C(3)-O(3) 1.177(4), C(4)-N(1) 1.458(4), C(4)-C(5) 1.473(4), C(5)-N(2) 1.152(5), Ru(1)-C(1)-O(1) 174.8(3), Ru(2)-C(2)-O(2) 176.2(3), Ru(1)-C(3)-Ru(3) 83.59(13), Ru(1)-C(4)-Ru(2) 80.18(11), C(5)-C(4)-N(1) 112.4(3), C(4)-C(5)-N(2) 178.7(4), C(4)-N(1)-C(6) 112.1(3), C(4)-N(1)-C(7) 116.0(3), C(6)-N(1)-C(7) 113.1(3).

The IR spectrum of **7aRu** (in CH_2Cl_2) exhibits the pattern typical of a $Ru_2Cp_2(CO)_2(\mu\text{-}CO)$ core, consisting of three carbonyl bands (2004, 1968 and 1800 cm^{-1}, respectively). Additionally, the absorption at 2146 cm^{-1} accounts for the carbene-bound cyano moiety. The NMR spectra ($CDCl_3$) reveals the presence of a single species in solution, likely corresponding to the same geometry observed in the solid-state structure, thereby indicating the absence of stereoisomerism arising from the orientation of the Cp ligands or the alkylidene substituent. The ^{13}C NMR signal for the alkylidene carbon falls at 139.8 ppm, consistent with data on related diruthenium complexes [34,68].

Surprisingly, the reaction of the diiron counterpart of **3aRu**, namely **3aFe**, with cyanide revealed significant differences between these two homologous compounds (Scheme 4). A mixture of products was obtained from **3aFe**, as indicated by the IR spectrum of the reaction mixture. Through careful chromatography under a strictly inert atmosphere, the alkylidene complex **7aFe** and the aminocarbyne derivative **8aFe** were separated. The unprecedented **7aFe** proved to be strongly air-sensitive, converting upon air contact into **3aFe** (detected by IR and ^1H analyses) and a paramagnetic mixture of unidentified carbonyl species. Moreover, **7aFe** is unstable in CH_2Cl_2 or $CDCl_3$, where it slowly underwent cyanide loss to recover **3aFe**, presumably via cyanide–chloride exchange with the solvent [69]. Thus, the identification of **7aFe** relied on the solution IR spectrum and key NMR data, but a full spectroscopic characterization was not possible.

Complex **8aFe** was previously synthesized from **3aFe** using the acetonitrile substitution route (see Scheme 1) [36,70]. Diiron and diruthenium complexes with the general formula $[M_2Cp_2(L)(CO)(\mu\text{-}CO)\{\mu\text{-}CN(Me)(R)\}]^{0/+}$ (R ≠ Me, L = anionic or neutral ligand) can exhibit both cis/trans isomers, with reference to the geometry of the Cps, and α/β isomers, differing in the relative orientation of R and L [7,8,70], as shown in Scheme 5. The α/β isomerism arises from the inhibited rotation around the μ-(C-N) bond, which possesses a significant iminium character [8]. When L is a halide or pseudohalide ligand, the IR

spectrum serves as a strongly diagnostic tool for detecting cis and trans forms. Typically, the bridging CO stretching wavenumber (around 1800 cm^{-1}) is almost coincident in such two isomers, while the terminal CO stretching significantly differs, occurring at ca. 1980 and 1960 cm^{-1} in the cis and trans isomers, respectively [7,8,70].
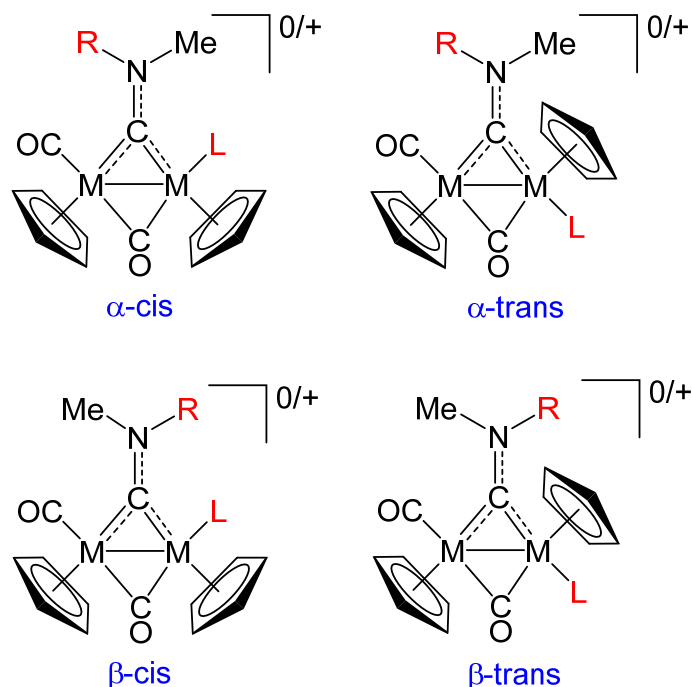
Scheme 5. α/β and cis/trans isomers observed in asymmetric diiron and diruthenium aminocarbyne complexes. R = aryl or alkyl $\neq$ Me. L = anionic or neutral ligand, corresponding to neutral and cationic complexes, respectively.

The IR and ^{1}H NMR spectra of **8aFe** indicate the presence in solution of α-trans and β-trans isomers, as previously reported [70].

The outcome of the reaction involving **3aFe** contrasts with previous findings where **3bFe** reacted with tetrabutylammonium cyanide yielding the cyano-alkylidene derivative **7bFe** as the sole, stable product [33]. The steric hindrance introduced by the cyclohexyl group in **3aFe** presumably plays a crucial role in disfavoring cyanide binding to the carbyne [20], although electronic factors should also be invoked, given the discrepancy observed between the reactivities of **3aFe** and **3aRu**.

To test the thermodynamic stability of the cyano-alkylidene complexes **7bFe** and **7aRu**, these were subjected to thermal treatment in various solvents. Interestingly, **7bFe** underwent quantitative conversion to **8bFe** when heated at around 60 °C in isopropanol, acetonitrile or tetrahydrofuran solutions. This conversion involved CO elimination and intramolecular cyanide migration. Isopropanol proved to be the most effective solvent for this transformation, yielding **8bFe** in a 71% yield.

The IR spectrum of the reaction mixture revealed that the cyanide migration was nonselective when conducted in THF solution, resulting in the production of **8bFe** in combination with minor, unidentified species. Note that the CO and Cp rings are potential sites of the addition of carbon nucleophiles to dinuclear complexes of type **3** [71,72].

Complex **8bFe**, previously obtained via either CO-NCMe substitution (Scheme 1) [35] or selenocyanate decomposition [70], was identified by comparing spectroscopic data with the literature. The structure of **8bFe** (as the bis-aqua species trans-**8bFe·2H₂O**) was confirmed by X-ray diffraction (Figure S4). The structure of trans-**8bFe** was previously reported as a solvent-free crystal [70]. Bonding parameters and stereochemistry are almost identical and will not be commented on any further. Hydrogen bonds are present involving the cyanide ligand and the water molecules. The only other example of crystallographically

characterized dimetallic bis-cyclopentadienyl carbonyl complex featuring a terminal CN ligand is the homolog of **8bFe** exhibiting two cis-oriented methylcyclopentadienyl ligands (Cp′) [73].

The IR spectrum of **8bFe** is diagnostic for a mixture of cis and trans isomers, with a prevalence of the former (CO bands at 1980, 1958 and 1803 cm^{-1}, vide infra) [8,70]. Consistently, the ^{1}H NMR spectrum revealed two sets of signals in an approximate 4.5 ratio.

The diruthenium complex **7aRu** was sluggish to the CN$^-$ migration–CO removal process described for **7bFe**. As a matter of fact, this reaction reached approximately 50% conversion after 24 h in isopropanol at reflux. Adding TMNO to the reaction mixture significantly accelerated the process, reaching completion after 30 min in isopropanol at 60 °C. However, the favorable action of TMNO was at the expense of selectivity, resulting in significant amounts of a secondary product. Following alumina chromatography, **8aRu** was finally isolated in a moderate yield. We explored the alternative possibility of obtaining **8aRu** via chloride–cyanide replacement, similar to the process described for the synthesis of **6** from **2Ru-Cl** (see Scheme 3). However, this route proved impracticable, as **3aRu-Cl** showed inertness towards Bu$_4$NCN (Scheme 4).

The carbonyl pattern in the IR spectrum of **8aRu** suggests the presence of trans and cis isomers, with a large prevalence of the former, revealing a prevalent cis to trans rearrangement of the Ru$_2$Cp$_2$ scaffold ongoing from **7aRu** to **8aRu**. The infrared absorption for the cyano group falls at 2098 cm^{-1}, suggestive of a Ru-CN linkage. Moreover, the aminocarbyne μ-C-N bond manifests itself with a medium intensity band at 1540 cm^{-1}, consistent with its partial double bond character [8,21].

The ^{1}H NMR spectrum of **8aRu** exhibits two sets of signals for each cis/trans species, attributable to the α and β forms (Scheme 5). The overall trans to cis ratio is approximately 6. In the ^{13}C NMR spectrum, the carbyne center resonates in the typical low-field region characteristic of dinuclear μ-aminocarbyne complexes [8,74–76]. A comparative view of spectroscopic features of **8aRu** and **8aFe** (Table 1) highlights important electronic effects provided by the distinct metal centers. Regarding the IR signals, they are slightly shifted to lower wavenumbers in **8aFe** compared to **8aRu**. This observation is coherent with the generally higher degree of π-backdonation occurring to π-acceptor ligands from 3d soft metal centers compared to their 4d congeners, correlated with the lower electronegativity of the 3d elements, resulting in stronger 3d metal–ligand bonds [77–80].

Table 1. Comparative view of IR (CH$_2$Cl$_2$ solutions) and NMR (CDCl$_3$ solutions) data for trans-**8aFe** [70] and trans-**8aRu** (this work). NMR data refer to the prevalent α isomers (see Scheme 5).
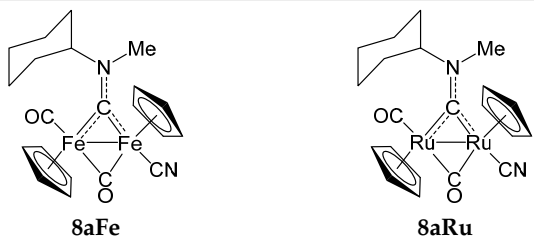

	8aFe	8aRu
IR (CH$_2$Cl$_2$), $\tilde{v}$/cm^{-1}		
CO (terminal)	1959	1962
CO (bridging)	1803	1804
C≡N	2089	2098
m-CN	1528	1540
^{1}H NMR (CDCl$_3$), δ/ppm		
Cp	4.80, 4.64	5.32, 5.20
N-Me	4.04	3.76

Table 1. *Cont.*

| ¹³C NMR (CDCl₃), δ/ppm		
CO (terminal)	262.2	232.6
CO (bridging)	212.6	199.3
m-CN	336.1	303.8
Cp	90.2, 90.0	91.5, 90.0
N-Me	44.2	45.4
C≡N	140.6	143.3

3. Experimental Section

3.1. General Details

Complexes $[M_2Cp_2(CO)_4]$ (M = Fe, Ru) were purchased from Merck, while organic reagents were purchased from Merck or TCI Europe, and were of the utmost available purity. Complexes **1Ru-NCMe** [25], **1Fe** [16], **2-NCMe** [27], **2Ru-Cl** [27], **3aRu** [22], **3aFe** [21], **3bFe** [20], **7bFe** [33] were prepared according to the literature. Solvents were obtained from Merck (petroleum ether with a boiling point range of 40–60 °C). Dichloromethane, acetonitrile, tetrahydrofuran and hexane underwent drying using the solvent purification system mBraun MB SPS5. Reactions were carried out under N_2 atmosphere using standard Schlenk techniques and anhydrous solvents, and were monitored through liquid infrared spectroscopy. Chromatographic separations were conducted on columns of deactivated alumina (Merck, 4% *w/w* water) under N_2 atmosphere, using solvents from the bottle. Infrared spectra of solutions were recorded on a Perkin Elmer Spectrum 100 FT-IR spectrometer with a CaF_2 liquid transmission cell (2300–1500 cm^{-1} range). IR spectra were processed with Spectragryph software [81]. NMR spectra were recorded at 298 K on a Jeol JNM-ECZ 400 MHz or a Jeol JNM-ECZ500R instrument, both equipped with Royal HFX Broadband probe. Chemical shifts (expressed in parts per million) are referenced to the residual solvent peaks (¹H, ¹³C) [82]. NMR spectra were assigned with the assistance of ¹H-¹³C (*gs*-HSQC and *gs*-HMBC) correlation experiments [83]. NMR signals due to secondary isomeric forms (where detectable) are italicized. Elemental analyses were performed on solid samples washed with pentane and prolongedly dried under vacuum, using a Vario MICRO cube instrument (Elementar). The isolated products were conserved under N_2 atmosphere.

3.2. Reaction of Diiron μ-Allenyl Complex (*1Fe*) with Bu₄NCN: Formation of [Fe₂Cp₂(CO)(μ-CO){μ,η¹:η³-CH=C(MeC=CH₂)C=O}] (*4, Figure 5*)

A solution of **1Fe** (107 mg, 0.223 mmol) in CH_2Cl_2 (10 mL) was treated with Bu_4NCN (66 mg, 0.246 mmol) and then left to stir for 3 h. The final solution was loaded on top of an alumina column, and the brown fraction corresponding to **4** was collected using a mixture of CH_2Cl_2 and THF (1:1 *v/v*) as the eluent. This product was obtained as a brown solid upon solvent evaporation under vacuum. Yield 44 mg, 50%. IR (CH_2Cl_2): ṽ/cm^{-1} = 1975vs (CO), 1796s (μ-CO), 1748m (C=O), 1611m (C=C).
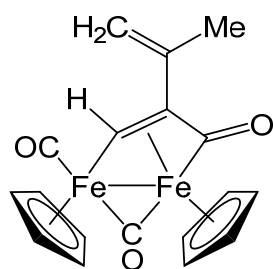
Figure 5. Structure of **4**.

3.3. Reaction of Diruthenium μ-Allenyl Complex (1Ru-NCMe) with Bu₄NCN: Synthesis and Isolation of [Ru₂Cp₂(CO)₂{μ,η²:η²-CH(CN)=C=CMe₂}] (5A, Figure 6), Identification of [Ru₂Cp₂(CN)(CO)(μ-CO){μ,η¹:η²-CH=C=CMe₂}] (5B1, 5B2, Figure 6)

A solution of **1Ru-NCMe**, freshly prepared from **1Ru** (118 mg, 0.207 mmol), in CH₂Cl₂ (10 mL) was treated with Bu₄NCN (69 mg, 0.257 mmol). The resulting mixture was left to stir for 40 min, until it turned dark yellow. The final solution was loaded on top of an alumina column. A pale-yellow fraction was collected using neat dichloromethane as the eluent and corresponded to **5A**. Subsequently, the second fraction (yellow) was isolated using a CH₂Cl₂/THF mixture (1/1 *v/v*), corresponding to a mixture of **5B1** and **5B2** contaminated with tetrabutylammonium. The solvent was evaporated from each solution under vacuum.
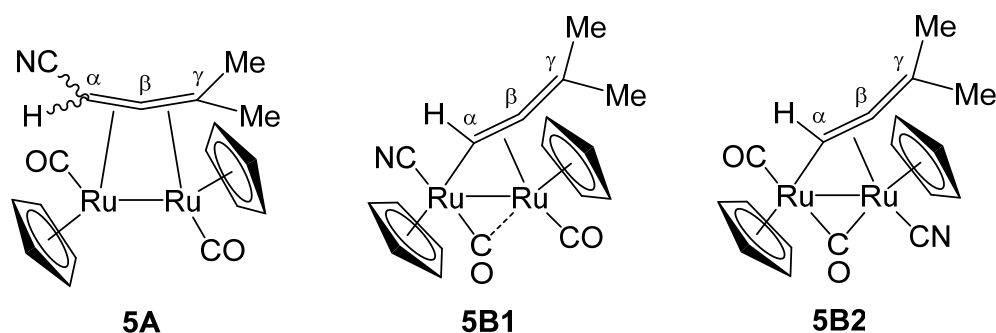
Figure 6. Structures of **5A**, **5B1** and **5B2** (wavy bonds indicate stereoisomerism).

5A. Yellow solid, yield 27 mg (27%). Anal. calcd. for C₁₈H₁₇NO₂Ru₂: C, 44.90; H, 3.56; N, 2.91. Found: C, 44.65; H, 3.64; N, 2.80. IR (CH₂Cl₂): ṽ/cm⁻¹ = 2200w (C≡N), 1948s (CO), 1928vs (CO). ¹H NMR (CDCl₃): δ/ppm = 5.11, *5.11*, 5.08, *4.83* (s, 10H, Cp); *3.45*, 2.47 (s, 1H, CₐH); 2.07, *2.00*, 1.92, *1.79* (s, 6H, Me). ¹³C{¹H} NMR (CDCl₃): δ/ppm = 207.7, *206.3*, *206.2*, 206.1 (CO); 189.8, *189.0* (C_β); *125.8*, 125.2 (C≡N); *87.8*, 87.1, 85.9, *85.9* (Cp); 65.4, *64.1* (C_γ); *36.0*, 35.7, 32.6, *32.5* (Me); *5.69*, 5.32 (Cₐ). Isomer ratio ≈ 1.7.

5B1 + 5B2. Ochre-yellow solid, yield ≈56 mg (56%). IR (CH₂Cl₂): ṽ/cm⁻¹ = 2104w-br (C≡N), 1983vs (CO), 1894m (μ-CO), 1827w (μ-CO). ¹H NMR (CDCl₃): δ/ppm = *9.44*, 9.06 (m, 1H, CₐH); *5.30*, 5.26, *5.15*, 5.08 (s, 10H, Cp); 2.29, 2.23, *1.98*, 1.88 (d, 3H, ³J_HH = 2.2 Hz, Me). **5B1/5B2** ratio ≈ 3.3.

The mixture of **5B1** and **5B2** was cleanly converted into **5A** upon heating in heptane solution at reflux temperature for 2h. Afterwards, complex **5A** was purified by alumina chromatography and finally isolated as a yellow solid with a total yield of 60%.

3.4. Reaction of Diruthenium μ-Vinyl Complex (2Ru-Cl) with Bu₄NCN: Synthesis of [Ru₂Cp₂(CN)(CO)(μ-CO){μ,η¹:η²-C(Ph)=CHPh}] (6, Figure 7)

*3.4. Reaction of Diruthenium μ-Vinyl Complex (**2Ru-Cl**) with Bu₄NCN: Synthesis of [Ru₂Cp₂(CN)(CO)(μ-CO){μ,η¹:η²-C(Ph)=CHPh}] (**6**, Figure 7)*

A dark-orange solution of **2Ru-Cl** (25 mg, 0.041 mmol) in CH₂Cl₂ (10 mL) was treated with Bu₄NCN (14 mg, 0.052 mmol). The resulting mixture was left to stir for 1.5 h, and the final light-orange solution was loaded on top of an alumina column. The fraction corresponding to **6** was collected using a CH₂Cl₂/THF mixture (3/1 *v/v*). The title compound was obtained as a yellow solid upon solvent evaporation under vacuum. Yield 20 mg (84%). Anal. calcd. for C₂₇H₂₁NO₂Ru₂: C, 54.63; H, 3.57; N, 2.36. Found: C, 54.29; H, 3.45; N, 2.49. IR (CH₂Cl₂): ṽ/cm⁻¹ = 2104w (C≡N), 1978vs (CO), 1826s (μ-CO). ¹H NMR (CDCl₃): δ/ppm = 7.30, 7.19, 7.06, 6.96 (m, 10H, Ph); 5.38, 4.97 (s, 10H, Cp); 4.92 (s, 1H, C_βH). ¹³C{¹H} NMR (CDCl₃): δ/ppm = 226.3, 198.3 (CO); 174.6 (*ipso*-Ph); 154.4 (Cₐ); 143.4 (*ipso*-Ph); 132.6 (C≡N); 129.1, 128.6, 128.5, 128.2, 126.7, 126.1 (Ph); 93.3, 93.0 (Cp); 72.4 (C_β).
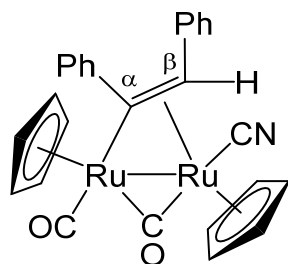
Figure 7. Structure of **6**.

3.5. Reactions of Diiron and Diruthenium μ-Aminocarbyne Complexes (3) with Bu₄NCN

3.5.1. Synthesis of [Ru$_2$Cp$_2$(CO)$_2$(μ-CO){μ-C(CN)N(Me)(Cy)}] (**7aRu**, Figure 8)

A pale-yellow solution of **3aRu** (90 mg, 0.131 mmol) in CH$_2$Cl$_2$ (7 mL) was treated with Bu$_4$NCN (39 mg, 0.15 mmol). The solution turned immediately orange and was left to stir for an additional 30 min. Subsequently, the solution was filtered through an alumina column using neat dichloromethane as the eluent. The title compound was obtained as an orange solid upon solvent evaporation under vacuum. Yield 55 mg (74%). Anal. calcd. for C$_{22}$H$_{24}$N$_2$O$_3$Ru$_2$: C, 46.64; H, 4.27; N, 4.94. Found: C, 46.25; H, 4.15; N, 5.03. IR (CH$_2$Cl$_2$): $\tilde{v}$/cm^{-1} = 2146w (C≡N), 2004vs (CO), 1968m (CO), 1800s (μ-CO). ^{1}H NMR (CDCl$_3$): δ/ppm = 5.23 (s, 10H, Cp); 3.35 (m, 1H, CH^{Cy}); 2.75 (s, 3H, Me); 2.02, 1.81, 1.62, 1.37, 1.24 (m, 10H, CH$_2$^{Cy}). ^{13}C{^{1}H} NMR (CDCl$_3$): δ/ppm = 229.2 (μ-CO); 196.1, 195.5 (CO); 139.8 (μ-CN); 130.3 (C≡N); 92.7 (Cp); 70.1 (CH^{Cy}); 38.8 (Me); 29.7, 26.9, 26.4 (CH$_2$^{Cy}). Crystals of **7aRu·CH$_2$Cl$_2$** suitable for X-ray analysis were obtained by slow diffusion of dichloromethane into a hexane solution of **7aRu**, at −30 °C.
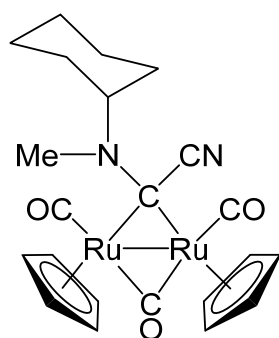
**Figure 8.** Structure of **7aRu**.

3.5.2. Formation of [Fe$_2$Cp$_2$(CO)$_2$(μ-CO){μ-C(CN)N(Me)Cy}] (**7aFe**, Figure 9) and [Fe$_2$Cp$_2$(CN)(CO)(μ-CO){μ-CN(Me)Cy}] (**8aFe**, Figure 9)

A red solution of **3aFe** (100 mg, 0.188 mmol) in CH$_2$Cl$_2$ (7 mL) was treated with Bu$_4$NCN (58 mg, 0.22 mmol) and stirred for 1 h. The resulting solution was analyzed by IR spectroscopy [$\tilde{v}$/cm^{-1} = 2142w, 2090w, 2068m, 2002vs, 1945s, 1796m, 1739s] and then loaded on top of an alumina column. Elution with neat dichloromethane afforded a purple fraction corresponding to **7aFe**. Subsequently, a dark-green fraction corresponding to **8aFe** was collected using acetonitrile as the eluent. The solvent was evaporated from each solution under vacuum.

7aFe. Purple solid, yield 31 mg (35%). IR (CH$_2$Cl$_2$): $\tilde{v}$/cm^{-1} = 2142w (C≡N), 2002vs (CO), 1966m (CO), 1796w (μ-CO). ^{1}H NMR (CDCl$_3$): δ/ppm = 5.46, 5.34 (s, 10H, Cp); 3.36 (m, 1H, CH^{Cy}); 2.56 (s, 3H, NMe); 1.97–1.20 (m, 10H, CH$_2$^{Cy}). Complex **7aFe** completely decomposed in a few hours when stored in air or in a CH$_2$Cl$_2$ or CDCl$_3$ solution, yielding [Fe$_2$Cp$_2$(CO)$_2$(μ-CO){μ-CN(Me)Cy}]$^+$ as the main species. AgNO$_3$ test on a methanol solution of the degradation mixture resulted in abundant precipitation of a white solid (AgCl).
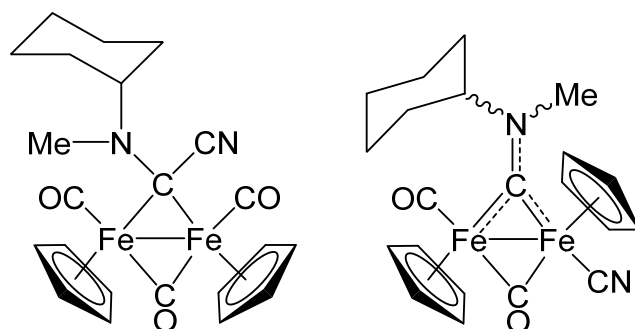
Figure 9. Structures of **7aFe** and **8aFe** (wavy bonds indicate stereoisomerism).

8aFe. Green solid, in admixture with [Bu$_4$N]CF$_3$SO$_3$ (**8a**/Bu$_4$N ratio ≈ 1). Yield 31 mg (37%). IR (CH$_2$Cl$_2$): ṽ/cm^{-1} = 2089w (C≡N), 1959vs (CO), 1803s (μ-CO), 1528w (μ-CN). ^{1}H NMR (CDCl$_3$): δ/ppm = 5.33, *5.13* (m, 1 H, CH^{Cy}); 4.80, *4.78*, *4.65*, 4.64 (s, 10 H, Cp); *4.17*, 4.04 (s, 3 H, NMe); 2.27–2.17, 2.10–1.83, 1.64, 1.34–1.24 (m, 10 H, CH$_2$^{Cy}). Stereoisomer ratio (α/β) ≈ 2.4.

3.6. Thermal Decarbonylation Reactions

3.6.1. Synthesis of [Fe$_2$Cp$_2$(CN)(CO)(μ-CO){μ-CN(Me)$_2$}] (**8bFe**, Figure 10)

A solution of **7bFe** (70 mg, 0.13 mmol) in deaerated ^{i}PrOH (10 mL) was heated at 60 °C for 1 h. Afterwards, the volatiles were removed under vacuum, and the resulting residue was dissolved in the minimum volume of dichloromethane. A larger volume of diethyl ether was added to the solution, affording a precipitate which was isolated and dried under vacuum. Green-brown solid, yield 36 mg (71%). IR (CH$_2$Cl$_2$): ṽ/cm^{-1} = 2091m (C≡N), 1980vs (CO), 1958s-sh (CO), 1803s (μ-CO), 1578m (μ-CN). ^{1}H NMR (CDCl$_3$): δ/ppm = *4.84*, 4.80, 4.77, *4.71* (s, 5H, Cp); *4.34*, 4.25, *4.21*, 4.11 (s, 3H, Me). Isomer ratio (cis/trans) ≈ 4.5. Crystals of trans-**8bFe·2H$_2$O** suitable for X-ray analysis were obtained by slow evaporation of the solvent from a solution of **8bFe** in a dichloromethane/hexane mixture, in contact with air.
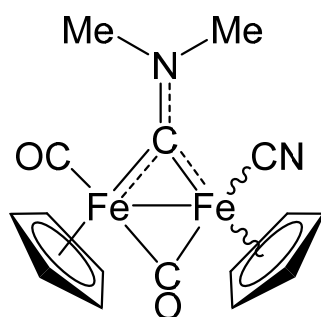
Figure 10. Structure of **8bFe** (wavy bonds indicate stereoisomerism).

3.6.2. Synthesis of [Ru$_2$Cp$_2$(CN)(CO)(μ-CO){μ-CN(Me)(Cy)}] (**8aRu**, Figure 11)

A mixture of **7aRu** (55 mg, 0.097 mmol) and Me$_3$NO·2H$_2$O (TMNO·2H$_2$O; 12 mg, 0.11 mmol) in deaerated ^{i}PrOH (10 mL) was heated at 80 °C for 2 h. Afterwards, the volatiles were removed under vacuum, and the resulting residue was dissolved in the minimum volume of dichloromethane. This solution was loaded on top of an alumina column. Impurities were eluted using dichloromethane. Subsequently, the yellow fraction corresponding to the title product was collected using a CH$_2$Cl$_2$/THF mixture (1:1 *v/v*). The solvent was then evaporated under vacuum, affording a yellow solid. Yield 25 mg (48%). Anal. calcd. for C$_{21}$H$_{24}$N$_2$O$_2$Ru$_2$: C, 46.83; H, 4.49; N, 5.20. Found: C, 46.58; H, 4.39; N, 5.16. IR (CH$_2$Cl$_2$): ṽ/cm^{-1} = 2098w (C≡N), ~1980w-sh, 1962vs (CO), 1804s (μ-CO), 1540m (μ-CN).
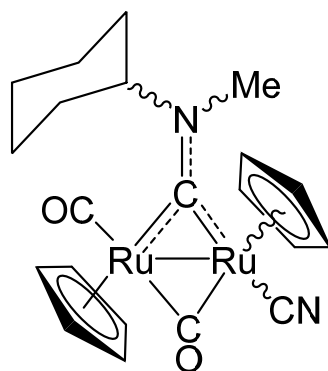
Figure 11. Structure of **8aRu** (wavy bonds indicate stereoisomerism).

trans-8aRu. ^{1}H NMR (CDCl$_3$): δ/ppm = *5.33*, 5.32, *5.21*, 5.20 (s, 10H, Cp); *4.87–4.78*, 4.74–4.66 (m, 1H, CH^{Cy}); 3.76, *3.76* (s, 3H, Me); 2.03–1.68 (m, 10H, CH$_2^{Cy}$). ^{13}C{^{1}H} NMR (CDCl$_3$): δ/ppm = *304.0*, 303.8 (μ-CN); 232.6, *229.5* (μ-CO); 199.3 (CO); 143.3 (C≡N); 91.5, *91.3*, *90.2*, 90.0 (Cp); *76.4*, 76.0 (CH^{Cy}); 45.4, *44.7* (Me); 31.6–25.3 (CH$_2^{Cy}$). Isomer ratio (α/β) ≈ 1.1.

cis-8aRu. ^{1}H NMR (CDCl$_3$): δ/ppm = 5.24, *5.22*, 5.20, *5.19* (s, 10H, Cp); 3.73, *3.69* (s, 3H, Me); 2.03–1.68 (m, 10H, CH$_2^{Cy}$). ^{13}C{^{1}H} NMR (CDCl$_3$): δ/ppm = *88.6*, 88.5, 88.5, *88.4* (Cp). Isomer ratio ≈ 1.1. Global trans/cis ratio (α/β) ≈ 6.

3.7. Attempt to Prepare 8aRu via Chloride–Cyanide Substitution

The chloride complex **3aRu-Cl** was prepared using a procedure analogous to that reported for the synthesis of the homologous diiron compound [21]. A mixture of **3aRu** (70 mg, 0.10 mmol), Me$_3$NO·2H$_2$O (TMNO·2H$_2$O; 23 mg, 0.20 mmol) and LiCl (13 mg, 0.31 mmol) was refluxed in ^{i}PrOH (5 mL) for 2 h. The resulting red solution was allowed to cool to room temperature and taken to dryness under vacuum. Subsequently, **3aRu-Cl** was recovered from alumina column chromatography using THF as the eluent. The eluate was taken to dryness under vacuum and the resulting orange solid was washed with hexane and dried. Yield: 62 mg, 87%. Anal. Calcd. for C$_{20}$H$_{24}$ClNO$_2$Ru$_2$: C, 43.84; H, 4.41; N, 2.56. Found: C, 43.65; H, 4.28; N, 2.49. IR (CH$_2$Cl$_2$): ṽ/cm^{-1} = 1972s (CO), 1796s (μ-CO), 1545m (μ-CN). Then, a solution of **3aRu-Cl** (30 mg, 0.055 mmol) and Bu$_4$NCN (22 mg, 0.082 mmol) in dichloromethane (8 mL) was left to stir at room temperature for 4 h. Analysis via IR spectroscopy of the resulting mixture revealed the absence of any conversion.

4. X-ray Crystallography

Crystal data and collection details for **7aRu·CH$_2$Cl$_2$** and trans-**8bFe·2H$_2$O** are reported in Table 2. Data were recorded on a Bruker APEX II diffractometer equipped with a PHOTON2 detector using Mo–Kα radiation. Data were corrected for Lorentz polarization and absorption effects (empirical absorption correction SADABS) [84]. The structures were solved by direct methods and refined by full-matrix least-squares based on all data using F^2 [85]. Hydrogen atoms were fixed at calculated positions and refined by a riding model, excepts those of the water molecules of trans-**8bFe·2H$_2$O** which were located in the Fourier difference map and refined isotropically with restraints on the O-H and H···H distances. All non-hydrogen atoms were refined with anisotropic displacement parameters.

Table 2. Crystal data and measurement details for **7aRu·CH$_2$Cl$_2$** and trans-**8bFe·2H$_2$O**.

	7aRu·CH$_2$Cl$_2$	**trans-8bFe·2H$_2$O**
Formula	C$_{23}$H$_{26}$Cl$_2$N$_2$O$_3$Ru$_2$	C$_{16}$H$_{20}$Fe$_2$N$_2$O$_4$
FW	651.50	416.04
T, K	100(2)	100(2)
λ, Å	0.71073	0.71073
Crystal system	Monoclinic	Triclinic

Table 2. *Cont.*

	7aRu·CH₂Cl₂	trans-8bFe·2H₂O
Space group	C2/c	$P\bar{1}$
a, Å	23.6049(17)	7.1749(15)
b, Å	11.0767(8)	8.0419(17)
c, Å	18.9574(14)	14.623(3)
α, °	90	92.379(9)
β, °	98.353(3)	96.023(9)
γ, °	90	106.019(9)
Cell Volume, Å^3	4904.1(6)	804.3(3)
Z	8	2
D_c, g·cm^{-3}	1.765	1.718
μ, mm^{-1}	1.477	1.827
F(000)	2592	428
Crystal size, mm	$0.21 \times 0.19 \times 0.14$	$0.15 \times 0.11 \times 0.08$
θ limits, °	1.744–27.998	2.642–24.993
Reflections collected	34,456	5435
Independent reflections	5925 [R_{int} = 0.0503]	2799 [R_{int} = 0.0558]
Data/restraints/parameters	5925/71/300	2799/334/223
Goodness on fit on F$^{2\ a}$	1.031	1.127
R_1 ($I > 2\sigma(I)$) [b]	0.0353	0.0818
wR_2 (all data) [c]	0.0962	0.2074
Largest diff. peak and hole, e Å^{-3}	1.482/−1.560	1.961/−1.392

[a] Goodness on fit on F^2 = $[\sum w(F_O{}^2 - F_C{}^2)^2/(N_{ref} - N_{param})]^{1/2}$, where $w = 1/[\sigma^2(F_O{}^2) + (aP)^2 + bP]$, where $P = (F_O{}^2 + 2F_C{}^2)/3$; N_{ref} = number of reflections used in the refinement; N_{param} = number of refined parameters. [b] $R_1 = \sum \lVert F_O \rvert - \lvert F_C \rVert / \sum \lvert F_O \rvert$. [c] $wR_2 = [\sum w(F_O{}^2 - F_C{}^2)^2 / \sum w(F_O{}^2)^2]^{1/2}$, where $w = 1/[\sigma^2(F_O{}^2) + (aP)^2 + bP]$, where $P = (F_O{}^2 + 2F_C{}^2)/3$.

5. Details of DFT Calculations

All geometries were optimized with ORCA 5.0.3 [86] using the BP86 functional with the zero-order regular approximation (ZORA) to take relativistic effects into account and in conjunction with a triple-ζ quality basis set (ZORA-def2-TZVP) and the auxiliary basis set SARC/J. For ruthenium, the basis set "SARC-ZORA-TZVP" [87] was used. The dispersion corrections were introduced using the Grimme D3-parametrized correction and the Becke–Johnson damping to the DFT energy [88]. All the structures were confirmed to be local energy minima (no imaginary frequencies). The solvent was considered through the continuum-like polarizable continuum model (C-PCM, dichloromethane).

6. Conclusions

Dimetallic compounds offer uncommon reactivity enabled by cooperative effects provided by the interconnected metal centers, and diiron and diruthenium complexes based on the $M_2Cp_2(CO)_3$ scaffold serve as versatile substrates to explore reaction patterns and build new organometallic ligands. In this work, we explore the reactivity of a series of these types of complexes, featuring different hydrocarbyl ligands (C_xH_y) on one bridging site, towards the cyanide ion. We demonstrate that cyanide addition may be favored by the prior extrusion of one CO ligand, and can be directed to the metal centers or the C_xH_y fragment, depending on the cases. However, intramolecular cyanide migration, from one site to another, can be promoted thermally, and is facilitated by the flexibility of the $M_2Cp_2(CO)_n$ framework, where the Cp and CO ligands easily exchange their positions and spatial arrangements adapting to structural changes on the hydrocarbyl moiety. Interestingly, the reactivity of aminocarbyne complexes highlights a significant influence of the metal type, with the aminocarbyne moiety manifesting enhanced stability in diiron complexes compared to diruthenium homologues. Overall, our findings expand the knowledge on the reactivity of easily accessible organometallic platforms and may provide useful insights for future synthetic design and catalytic studies.

References

1. Campos, J. Bimetallic cooperation across the periodic table. *Nat. Rev. Chem.* **2020**, *4*, 696–702. [CrossRef] [PubMed]
2. Ritleng, V.; Chetcuti, M.J. Hydrocarbyl Ligand Transformations on Heterobimetallic Complexes. *Chem. Rev.* **2007**, *107*, 797–858. [CrossRef] [PubMed]
3. Govindarajan, R.; Deolka, S.; Khusnutdinova, J.R. Heterometallic bond activation enabled by unsymmetrical ligand scaffolds: Bridging the opposites. *Chem. Sci.* **2022**, *13*, 14008–14031. [CrossRef]
4. Patra, S.; Maity, N. Recent advances in (hetero)dimetallic systems towards tandem catalysis. *Coord. Chem. Rev.* **2021**, *434*, 213803. [CrossRef]
5. Knorr, M.; Jourdain, I. Activation of alkynes by diphosphine- and m-phosphido-spanned heterobimetallic complexes. *Coord. Chem. Rev.* **2017**, *350*, 217–247. [CrossRef]
6. Mazzoni, R.; Salmi, M.; Zanotti, V. C-C Bond Formation in Diiron Complexes. *Chem. Eur. J.* **2012**, *18*, 10174–10194. [CrossRef] [PubMed]
7. Marchetti, F. Constructing Organometallic Architectures from Aminoalkylidyne Diiron Complexes. *Eur. J. Inorg. Chem.* **2018**, 3987–4003. [CrossRef]
8. Biancalana, L.; Marchetti, F. Aminocarbyne ligands in organometallic chemistry. *Coord. Chem. Rev.* **2021**, *449*, 214203. [CrossRef]
9. Chen, J.; Wang, R. Remarkable reactions of cationic carbyne complexes of manganese, rhenium, and diiron with carbonylmetal anions. *Coord. Chem. Rev.* **2002**, *231*, 109–149. [CrossRef]
10. Busetto, L.; Maitlis, P.M.; Zanotti, V. Bridging vinylalkylidene transition metal complexes. *Coord. Chem. Rev.* **2010**, *254*, 470–486. [CrossRef]
11. Casey, C.P.; Marder, S.R.; Colborn, R.E.; Goodson, P.A. Conversion of Diiron Bridging Alkenyl Complexes to Monoiron Alkenyl Compounds and to Alkenes. *Organometallics* **1986**, *5*, 199–203. [CrossRef]
12. Casey, C.P.; Meszaros, M.W.; Fagan, P.J.; Bly, R.K.; Marder, S.R.; Austin, E.A. Hydrocarbation—Formation of Diiron μ-Alkylidyne Complexes from the Addition of the Carbon-Hydrogen Bond of a μ-Methylidyne Complex across Alkenes. *J. Am. Chem. Soc.* **1986**, *108*, 4043–4053. [CrossRef]
13. Bruce, G.C.; Knox, S.A.R.; Phillips, A.J. Synthesis of Butadiene via Vinyl-Ethylene Combination at a Diruthenium Centre. *J. Chem. Soc. Chem. Commun.* **1990**, 716–718. [CrossRef]
14. Turner, M.L.; Marsih, N.; Mann, B.E.; Quyoum, R.; Long, H.C.; Maitlis, P.M. Investigations by 13C NMR Spectroscopy of Ethene-Initiated Catalytic CO Hydrogenation. *J. Am. Chem. Soc.* **2002**, *124*, 10456–10472. [CrossRef]
15. Tsurugi, H.; Laskar, P.; Yamamoto, K.; Mashima, K. Bonding and structural features of metal-metal bonded homo- and hetero-dinuclear complexes supported by unsaturated hydrocarbon ligands. *J. Organomet. Chem.* **2018**, *869*, 251–263. [CrossRef]
16. Boni, A.; Marchetti, F.; Pampaloni, G.; Zacchini, S. Cationic Diiron and Diruthenium μ-Allenyl Complexes: Synthesis, X-ray Structures and Cyclization Reactions with Ethyldiazoacetate/Amine Affording Unprecedented Butenolide- and Furaniminium-Substituted Bridging Carbene Ligands. *Dalton Trans.* **2010**, *39*, 10866–10875. [CrossRef]
17. Bresciani, G.; Vančo, J.; Funaioli, T.; Zacchini, S.; Malina, T.; Pampaloni, G.; Dvořák, Z.; Trávníček, Z.; Marchetti, F. Anticancer Potential of Diruthenium Complexes with Bridging Hydrocarbyl Ligands from Bioactive Alkynols. *Inorg. Chem.* **2023**, *62*, 15875–15890. [CrossRef] [PubMed]
18. Bresciani, G.; Boni, S.; Funaioli, T.; Zacchini, S.; Pampaloni, G.; Busto, N.; Biver, T.; Marchetti, F. Adding Diversity to a Diruthenium Biscyclopentadienyl Scaffold via Alkyne Incorporation: Synthesis and Biological Studies. *Inorg. Chem.* **2023**, *62*, 12453–12467. [CrossRef] [PubMed]
19. Dyke, A.F.; Knox, S.A.R.; Morris, M.J.; Naish, P.J. Organic chemistry of dinuclear metal centres. Part 3. μ-Carbene complexes of iron and ruthenium from alkynes via μ-vinyl cations. *J. Chem. Soc. Dalton Trans.* **1983**, 1417–1426. [CrossRef]

20. Agonigi, G.; Bortoluzzi, M.; Marchetti, F.; Pampaloni, G.; Zacchini, S.; Zanotti, V. Regioselective Nucleophilic Additions to Diiron Carbonyl Complexes Containing a Bridging Aminocarbyne Ligand: A Synthetic, Crystallographic and DFT Study. *Eur. J. Inorg. Chem.* **2018**, 960–971. [CrossRef]

21. Biancalana, L.; De Franco, M.; Ciancaleoni, G.; Zacchini, S.; Pampaloni, G.; Gandin, V.; Marchetti, F. Easily Available, Amphiphilic Diiron Cyclopentadienyl Complexes Exhibit in Vitro Anticancer Activity in 2D and 3D Human Cancer Cells through Redox Modulation Triggered by CO Release. *Chem. Eur. J.* **2021**, *27*, 10169–10185. [CrossRef] [PubMed]

22. Vančo, J.; Fiaschi, M.; Biancalana, L.; Malina, T.; Dvořák, Z.; Funaioli, T.; Zacchini, S.; Guelfi, M.; Trávníček, Z.; Marchetti, F. An Exceptionally Aqueous Stable Diruthenium N-Indolyl Aminocarbyne Complex as a Prospective Anticancer Drug. *Inorg. Chem. Front.* **2024**, 1417–1426. [CrossRef]

23. Luh, T.Y. Trimethylamine N-Oxide-A Versatile Reagent for Organometallic Chemistry. *Coord. Chem. Rev.* **1984**, *60*, 255–276. [CrossRef]

24. Adams, K.J.; Barker, J.J.; Knox, S.A.R.; Orpen, A.G. Linking and fragmentation of alkynes at a triruthenium centre. *J. Chem. Soc. Dalton Trans.* **1996**, 975–988. [CrossRef]

25. Bresciani, G.; Zacchini, S.; Pampaloni, G.; Bortoluzzi, M.; Marchetti, F. η⁶-Coordinated ruthenabenzenes from three-component assembly on a diruthenium μ-allenyl scaffold. *Dalton Trans.* **2022**, *51*, 8390–8400. [CrossRef]

26. Bresciani, G.; Zacchini, S.; Pampaloni, G.; Marchetti, F. Carbon-Carbon Bond Coupling of Vinyl Molecules with an Allenyl Ligand at a Diruthenium Complex. *Organometallics* **2022**, *41*, 1006–1014. [CrossRef]

27. Bresciani, G.; Boni, S.; Zacchini, S.; Pampaloni, G.; Bortoluzzi, M.; Marchetti, F. Alkyne-alkenyl coupling at a diruthenium complex. *Dalton Trans.* **2022**, *51*, 15703–15715. [CrossRef] [PubMed]

28. Doherty, N.M.; Howard, J.A.K.; Knox, S.A.R.; Terrill, N.J.; Yates, M.I. Reactivity of Alkenes at a Diruthenium Centre: Combination with Methylene and Oxidative Activation. *J. Chem. Soc. Chem. Commun.* **1989**, 638–640. [CrossRef]

29. Pimparkar, S.; Koodan, A.; Maiti, S.; Ahmed, N.S.; Mostafa, M.M.M.; Maiti, D. C–CN bond formation: An overview of diverse strategies. *Chem. Commun.* **2021**, *57*, 22102232. [CrossRef]

30. Murahashi, S.-I.; Nakae, T.; Terai, H.; Komiya, N. Ruthenium-Catalyzed Oxidative Cyanation of Tertiary Amines with Molecular Oxygen or Hydrogen Peroxide and Sodium Cyanide: Sp³ C-H Bond Activation and Carbon—Carbon Bond Formation. *J. Am. Chem. Soc.* **2008**, *130*, 11005–11012. [CrossRef]

31. White, D.A.; Baizer, M.M. Tetra-alkylammonium Cyanides as Nucleophilic and Basic Reagents. *J. Chem. Soc. Perkin Trans.* **1973**, *1*, 2230–2236. [CrossRef]

32. Bartley, S.L.; Bernstein, S.N.; Dunbar, K.R. Acetonitrile and cyanide compounds containing metal-metal bonds: Syntheses, structures and applications to solid-state chemistry. *Inorg. Chim. Acta* **1993**, *213*, 213–231. [CrossRef]

33. Zanotti, V.; Bordoni, S.; Busetto, L.; Carlucci, L.; Palazzi, A.; Serra, R.; Albano, V.G.; Monari, M.; Prestopino, F.; Laschi, F.; et al. Diiron Aminoalkylidene Complexes. *Organometallics* **1995**, *14*, 5232–5241. [CrossRef]

34. Busetto, L.; Carlucci, L.; Zanotti, V.; Albano, V.G.; Monari, M. Ruthenium complexes with bridging functionalized alkylidene ligands. Synthesis of [Ru₂Cp₂(CO)₂(μ-CO){μ-C(X)N(Me)CH₂Ph}] (X = H, CN) and molecular structure of the CN derivative. *J. Organomet. Chem.* **1993**, *447*, 271–275. [CrossRef]

35. Albano, V.G.; Busetto, L.; Monari, M.; Zanotti, V. Reactions of acetonitrile di-iron μ-aminocarbyne complexes: Synthesis and structure of [Fe₂(μ-CNMe₂)(μ-H)(CO)₂(Cp)₂]. *J. Organomet. Chem.* **2000**, *606*, 163–168. [CrossRef]

36. Bresciani, G.; Biancalana, L.; Zacchini, S.; Pampaloni, G.; Ciancaleoni, G.; Marchetti, F. Diiron bis-cyclopentadienyl complexes as transfer hydrogenation catalysts: The key role of the bridging aminocarbyne ligand. *Appl. Organomet. Chem.* **2023**, *37*, e6990. [CrossRef]

37. Busetto, L.; Zanotti, V. Carbene ligands in diiron complexes. *J. Organomet. Chem.* **2005**, *690*, 5430–5440. [CrossRef]

38. Trylus, K.-H.; Kernbach, U.; Brüdgam, I.; Fehlhammer, W.P. Reaction patterns of 'tetraferrio-azaallenium', [(OC)₃Cp₂Fe₂(μ₄-CNC)Fe₂Cp₂(CO)₃]⁺, and its 'activated cyanide'-precursor (μ-phthalimidocarbyne)- tricarbonyldicyclopentadienyldiiron(1+). Inorg. *Chim. Acta* **1999**, *291*, 266–278.

39. Schoch, S.; Bresciani, G.; Saviozzi, C.; Funaioli, T.; Bortoluzzi, M.; Pampaloni, G.; Marchetti, F. Iminium Substituent Directs Cyanide and Hydride Additions to Triiron Vinyliminium Complexes. *New J. Chem.* **2023**, *47*, 8828–8844. [CrossRef]

40. Marchetti, F.; Zacchini, S.; Zanotti, V. Amination of Bridging Vinyliminium Ligands in Diiron Complexes: C-N Bond Forming Reactions for Amidine-Alkylidene Species. *Organometallics* **2018**, *37*, 107–115. [CrossRef]

41. Sulaiman, A.; Jiang, Y.-Z.; Khurram Javed, M.; Wu, S.-Q.; Li, Z.-Y.; Bu, X.-H. Tuning of spin-crossover behavior in two cyano-bridged mixed-valence Fe III2FeII trinuclear complexes based on a TpR ligand. *Inorg. Chem. Front.* **2022**, *9*, 241–248. [CrossRef]

42. Ghosh, P.; Quiroz, M.; Pulukkody, R.; Bhuvanesha, N.; Darensbourg, M.Y. Bridging cyanides from cyanoiron metalloligands to redox-active dinitrosyl iron units. *Dalton Trans.* **2018**, *47*, 11812–11819. [CrossRef] [PubMed]

43. Johansen, C.M.; Peters, J.C. Catalytic Reduction of Cyanide to Ammonia and Methane at a Mononuclear Fe Site. *J. Am. Chem. Soc.* **2024**, *146*, 5343–5354. [CrossRef] [PubMed]

44. Tard, C.; Pickett, C.J. Structural and Functional Analogues of the Active Sites of the [Fe]-, [NiFe]-, and [FeFe]-Hydrogenases. *Chem. Rev.* **2009**, *109*, 2245–2274. [CrossRef] [PubMed]

45. Fontecilla-Camps, J.C.; Volbeda, A.; Cavazza, C.; Nicolet, Y. Structure/Function Relationships of [NiFe]- and [FeFe]-Hydrogenases. *Chem. Rev.* **2007**, *107*, 4273–4303. [CrossRef] [PubMed]

46. Mazzoni, R.; Gabiccini, A.; Cesari, C.; Zanotti, V.; Gualandi, I.; Tonelli, D. Diiron Complexes Bearing Bridging Hydrocarbyl Ligands as Electrocatalysts for Proton Reduction. *Organometallics* **2015**, *34*, 3228–3235. [CrossRef]

47. Arrigoni, F.; Bertini, L.; De Gioia, L.; Cingolani, A.; Mazzoni, R.; Zanotti, V.; Zampella, G. Mechanistic Insight into Electrocatalytic H_2 Production by [Fe$_2$(CN){μ-CN(Me)$_2$}(μ-CO)(CO)(Cp)$_2$]: Effects of Dithiolate Replacement in [FeFe] Hydrogenase Models. *Inorg. Chem.* **2017**, *56*, 13852–13864. [CrossRef] [PubMed]

48. Arrigoni, F.; Bertini, L.; De Gioia, L.; Zampella, G.; Mazzoni, R.; Cingolani, A.; Gualandi, I.; Tonelli, D.; Zanotti, V. On the importance of cyanide in diiron bridging carbyne complexes, unconventional [FeFe]-hydrogenase mimics without dithiolate: An electrochemical and DFT investigation. *Inorg. Chim. Acta* **2020**, *510*, 119745. [CrossRef]

49. Knox, S.A.R.; Marchetti, F. Additions and intramolecular migrations of nucleophiles in cationic diruthenium μ-allenyl complexes. *J. Organomet. Chem.* **2007**, *692*, 4119–4128. [CrossRef]

50. Hoel, E.L.; Ansell, G.B.; Leta, S. Thermal and Photochemical Rearrangements of a Bridging Cyclopropylidene Ligand to Aliene In a Diiron Complex. *Organometallics* **1986**, *5*, 585–587. [CrossRef]

51. Al-Obaidi, Y.N.; Baker, P.K.; Green, M.; White, N.D.; Taylor, G.E. Reactions of co-ordinated ligands. Part 25. The synthesis of μ-allene-dicarbonylbis(η^5-indenyl)dirhodium and protonation to form a bridged cationic vinyl complex; molecular structures of μ-allene-dicarbonylbis(η^5-indenyl)dirhodium and dicarbonyl-bis(η^5-indenyl)-μ-(1-methylvinyl)-dirhodium(Rh–Rh) tetrafluoroborate. *J. Chem. Soc. Dalton Trans.* **1981**, 2321–2327. [CrossRef]

52. Wu, I.Y.; Tseng, T.W.; Chen, C.T.; Cheng, M.C.; Lin, Y.C.; Wang, Y. Synthesis of heterobimetallic allene complexes. *Inorg. Chem.* **1993**, *32*, 1539–1540. [CrossRef]

53. Justice, A.K.; Linck, R.C.; Rauchfuss, T.B. Diruthenium Dithiolato Cyanides: Basic Reactivity Studies and a Post Hoc Examination of Nature's Choice of Fe versus Ru for Hydrogenogenesis. *Inorg. Chem.* **2006**, *45*, 2406–2412. [CrossRef] [PubMed]

54. Darensbourg, D.J.; Lee, W.-Z.; Yarbrough, J.C. Synthesis and Characterization of a Monocyanide-Bridged Bimetallic Iron(II) and Copper(I) Complex. *Inorg. Chem.* **2001**, *40*, 6533–6536. [CrossRef] [PubMed]

55. Ruiz, M.S.; Romerosa, A.; Sierra-Martin, B.; Fernandez-Barbero, A. A Water Soluble Diruthenium–Gold Organometallic Microgel. *Angew. Chem. Int. Ed.* **2008**, *47*, 8665–8669. [CrossRef] [PubMed]

56. Doherty, S.; Hogarth, G.; Waugh, M.; Clegg, W.; Elsegood, M.R.J. Conversion of s,h-Allenyl Group into a s,s-(Diphenylphosphino)allyl and a Hexa-1,3,5-triene-2,6-diyl Ligand at a Diiron Center. *Organometallics* **2000**, *19*, 5696–5708. [CrossRef]

57. Dennett, J.N.L.; Knox, S.A.R.; Anderson, K.M.; Charmant, J.P.H.; Orpen, A.G. The synthesis of [FeRu(CO)$_2$(μ-CO)$_2$(Cp)(C$_5$Me$_5$)] and convenient entries to its organometallic chemistry. *Dalton Trans.* **2005**, 63–73. [CrossRef]

58. Dennett, J.N.L.; Knox, S.A.R.; Charmant, J.P.H.; Gillon, A.L.; Orpen, A.G. Synthesis and reactivity of m-butadienyl diruthenium cations. *Inorg. Chim. Acta* **2003**, *354*, 29–40. [CrossRef]

59. Biancalana, L.; Ciancaleoni, G.; Zacchini, S.; Pampaloni, G.; Marchetti, F. Carbonyl-isocyanide mono-substitution in [Fe$_2$Cp$_2$(CO)$_4$]: A re-visitation. *Inorg. Chim. Acta* **2020**, *517*, 120181. [CrossRef]

60. Guillevic, M.A.; Hancox, E.L.; Mann, B.E. A reinvestigation of the solution structure and dynamics of [Fe$_2$(η^5-C$_5$H$_5$)$_2$(CO)$_{4-n}$(CNMe)$_n$], n= 1 or 2. *J. Chem. Soc. Dalton Trans.* **1992**, 1729–1733. [CrossRef]

61. Adams, R.D.; Cotton, F.A. Low-valent metal isocyanine complexes. V. Structure and dynamical stereochemistry of bis(pentahaptocyclopentadienyl)tricarbonyl(tert-butyl isocyanide)diiron(Fe-Fe),(.eta.5-C$_5$H$_5$)$_2$Fe$_2$(CO)$_3$[CNC(CH$_3$)$_3$]. *Inorg. Chem.* **1974**, *13*, 257–262. [CrossRef]

62. Fehlhammer, W.P.; Schröder, A.; Schoder, F.; Fuchs, J.; Völkl, A.; Boyadjiev, B.; Schrölkamp, S. Synthese, Struktur und Dynamik van [Fe$_2$(CN)(Cp)$_2$(CO)$_3$]$^−$. *J. Organomet. Chem.* **1991**, *411*, 405–417. [CrossRef]

63. Jennings, M.C.; Puddephatt, R.J.; Manojlović-Muir, L.; Muir, K.W.; Mwariri, B.N. Binding modes of cyanide at trinuclear clusters. Crystal structure of [Pt$_3$(μ$_3$-CO)(CN)(dppm)$_3$][PF$_6$]. *Inorg. Chim. Acta* **1993**, *212*, 191–197. [CrossRef]

64. Hoffbauer, M.R.; Iluc, V.M. [2+2] Cycloadditions with an Iron Carbene: A Critical Step in Enyne Metathesis. *J. Am. Chem. Soc.* **2021**, *143*, 5592–5597. [CrossRef]

65. Bresciani, G.; Schoch, S.; Biancalana, L.; Zacchini, S.; Bortoluzzi, M.; Pampaloni, G.; Marchetti, F. Cyanide–alkene competition in a diiron complex and isolation of a multisite (cyano)alkylidene–alkene species. *Dalton Trans.* **2022**, *51*, 1936–1945. [CrossRef] [PubMed]

66. Biancalana, L.; Fiaschi, M.; Zacchini, S.; Marchetti, F. Formation and structural characterization of a diiron aminoalkylidene complex with N-cyano substituent. *Inorg. Chim. Acta* **2022**, *541*, 121093. [CrossRef]

67. Busetto, L.; Carlucci, L.; Zanotti, V.; Albano, V.G.; Braga, D. Synthesis, reactions, and X-ray structures of the functionalized isocyanide complexes [Fe$_2${μ-CNC(O)SR}(μ-CO)(CO)$_2$(cp)$_2$] (cp =η-C$_5$H$_5$, R = Me or Et) and of their carbyne and carbene derivatives. *J. Chem. Soc. Dalton Trans.* **1990**, 243–250. [CrossRef]

68. Albano, V.G.; Busetto, L.; Carlucci, L.; Cassani, M.C.; Monari, M.; Zanotti, V. Synthesis of dinuclear iron and ruthenium aminoalkylidene complexes and the molecular structure of the novel cis-[Ru$_2$(CO)$_2$(Cp)$_2${μ-C(CN)N(Me)Bz}$_2$](Cp = η-C$_5$H$_5$; Bz = CH$_2$Ph). *J. Organomet. Chem.* **1995**, *488*, 133–139. [CrossRef]

69. Friedman, L.; Shechter, H. Preparation of Nitriles from Halides and Sodium Cyanide. An Advantageous Nucleophilic Displacement in Dimethyl Sulfoxide. *J. Org. Chem.* **1960**, *25*, 877–879. [CrossRef]

70. Bresciani, G.; Zacchini, S.; Pampaloni, G.; Bortoluzzi, M.; Marchetti, F. Diiron Aminocarbyne Complexes with NCE$^−$ Ligands (E = O, S, Se). *Molecules* **2023**, *28*, 3251. [CrossRef]

71. Albano, V.G.; Busetto, L.; Camiletti, C.; Monari, M.; Zanotti, V. Further investigations on C-C bond formation at the diruthenium aminocarbyne complexes [Ru$_2${μ-CN(Me)R}(μ-CO)(CO)$_2$(Cp)$_2$]SO$_3$CF$_3$ (R = Me, CH$_2$Ph) and molecular structure of [Ru$_2$(μ-CNMe$_2$)(μ-CO)(COPh)(CO)(Cp)$_2$]. *J. Organomet. Chem.* **1998**, *563*, 153–159. [CrossRef]

72. Albano, V.G.; Busetto, L.; Camiletti, C.; Castellari, C.; Monari, M.; Zanotti, V. Selective C-C bond formation at diiron μ-aminocarbyne complexes. *J. Chem. Soc. Dalton Trans.* **1997**, 4671–4676. [CrossRef]

73. Boss, K.; Manning, A.R.; Muller-Bunz, H. The structure of the red-brown form of [Fe$_2$(η^5-C$_5$H$_4$Me)$_2$(CO)(CN)(μ-CO)(μ-CNMe$_2$)] and its confirmation as a cis isomer. *Z. Krist. Cryst. Mater.* **2006**, *221*, 266–269. [CrossRef]

74. Alvarez, M.A.; García, M.E.; García-Vivó, D.; Ruiz, M.A.; Vega, M.F. Insertion, Rearrangement, and Coupling Processes in the Reactions of the Unsaturated Hydride Complex [W$_2$(η^5-C$_5$H$_5$)$_2$(H)(μ-PCy$_2$)(CO)$_2$] with Isocyanides. *Organometallics* **2013**, *32*, 4543–4555. [CrossRef]

75. Knorr, M.; Strohmann, C. Syntheses, Structures, and Reactivity of Dinuclear Molybdenum-Platinum and Tungsten-Platinum Complexes with Bridging Carbonyl, Sulfur Dioxide, Isonitrile, and Aminocarbyne Ligands and a dppa Backbone (dppa)Ph$_2$PNHPPh$_2$). *Organometallics* **1999**, *18*, 248–257. [CrossRef]

76. Zhou, X.; Barton, B.E.; Chambers, G.M.; Rauchfuss, T.B. Preparation and Protonation of Fe$_2$(pdt)(CNR)$_6$, Electron-Rich Analogues of Fe$_2$(pdt)(CO)$_6$. *Inorg. Chem.* **2016**, *55*, 3401–3412. [CrossRef] [PubMed]

77. Basolo, F. Polyhedron report number 32: Kinetics and mechanisms of CO substitution of metal carbonyls. *Polyhedron* **1990**, *9*, 1503–1535. [CrossRef]

78. Fajardo, J.; Peters, J.C., Jr. Catalytic nitrogen-to-ammonia conversion by osmium and ruthenium complexes. *J. Am. Chem. Soc.* **2017**, *139*, 16105–16108. [CrossRef] [PubMed]

79. Ehlers, A.W.; Ruiz-Morales, Y.; Jan Baerends, E.; Ziegler, T. Dissociation Energies, Vibrational Frequencies, and ^{13}C NMR Chemical Shifts of the 18-Electron Species [M(CO)$_6$]$_n$ (M = Hf−Ir, Mo, Tc, Ru, Cr, Mn, Fe). A Density Functional Study. *Inorg. Chem.* **1997**, *36*, 5031–5036. [CrossRef]

80. Hughes, A.K.; Wade, K. Metal–metal and metal–ligand bond strengths in metal carbonyl clusters. *Coord. Chem. Rev.* **2000**, *197*, 191–229. [CrossRef]

81. Menges, F. "Spectragryph—Optical Spectroscopy Software", Version 1.2.5, @ 2016–2017. Available online: https://www.effemm2.de/spectragryph (accessed on 30 April 2024).

82. Fulmer, G.R.; Miller, A.J.M.; Sherden, N.H.; Gottlieb, H.E.; Nudelman, A.; Stoltz, B.M.; Bercaw, J.E.; Goldberg, K.I. NMR Chemical Shifts of Trace Impurities: Common Laboratory Solvents, Organics, and Gases in Deuterated Solvents Relevant to the Organometallic Chemist. *Organometallics* **2010**, *29*, 2176–2179. [CrossRef]

83. Willker, W.; Leibfritz, D.; Kerssebaum, R.; Bermel, W. Gradient selection in inverse heteronuclear correlation spectroscopy. *Magn. Reson. Chem.* **1993**, *31*, 287–292. [CrossRef]

84. Sheldrick, G.M. *SADABS-2008/1-Bruker AXS Area Detector Scaling and Absorption Correction*; Bruker AXS: Madison, WI, USA, 2008.

85. Sheldrick, G.M. Crystal structure refinement with SHELXL. *Acta Cryst. C* **2015**, *71*, 3. [CrossRef]

86. Neese, F. Software update: The ORCA program system—Version 5.0. *WIREs Comp. Mol. Sci.* **2022**, *12*, e1606. [CrossRef]

87. Rolfes, J.D.; Neese, F.; Pantazis, D.A. All-electron scalar relativistic basis sets for the elements Rb-Xe. *J. Comput. Chem.* **2020**, *41*, 1842. [CrossRef]

88. Grimme, S. Semiempirical GGA-type density functional constructed with a long-range dispersion correction. *J. Comput. Chem.* **2006**, *27*, 1787. [CrossRef]